

Chapter 5

Dynamics of Mitochondrial Redox and Energy Networks: Insights from an Experimental–Computational Synergy

Sonia Cortassa and Miguel A. Aon

Abstract Functionally, a cell comprises spatially distributed and compartmentalized subsystems, the dynamics of which occurs on several temporal scales. Interactivity in complex spatiotemporally organized cellular systems is fundamental to their counterintuitive behavior and one of the main reasons why their study needs mathematical modeling. But models alone are not enough; what we ultimately require is a combined experimental–theoretical approach in order to validate our models as rigorously as possible.

We explore in a detailed example the success of experimental–modeling synergy leading to the elucidation of the mechanisms involved in synchronized mitochondrial oscillations in the heart, and the discovery there of new related mechanisms. This work involves successive and iterative reciprocal potentiation of the loop via experiments and computational modeling: simulation–validation and prediction–experimentation thereby alternate so as to provide a deeper understanding of complex biological phenomena.

The concept of network has become central in systems biology. Conceptually, networks can be approached from different angles. One is *morphological*, in which mitochondrial spatial organization corresponds to a network because they exhibit a spatial arrangement with a defined pattern that *topologically* connects them in a certain way, for example, in a lattice as in cardiac cells, or reticular random as in neurons or cancer cells. However, underlying these networks there is another vast network of metabolic reactions with nodes represented by substrates, products, ion gradients, and links by enzymes catalyzing reactions between substrates and products, or transporters and channels modulating the passage of ions and metabolites across membranes. The metabolic network distributes among

S. Cortassa • M.A. Aon (✉)

Division of Cardiology, Johns Hopkins University, Baltimore, MD 21205, USA

e-mail: maon1@jhmi.edu

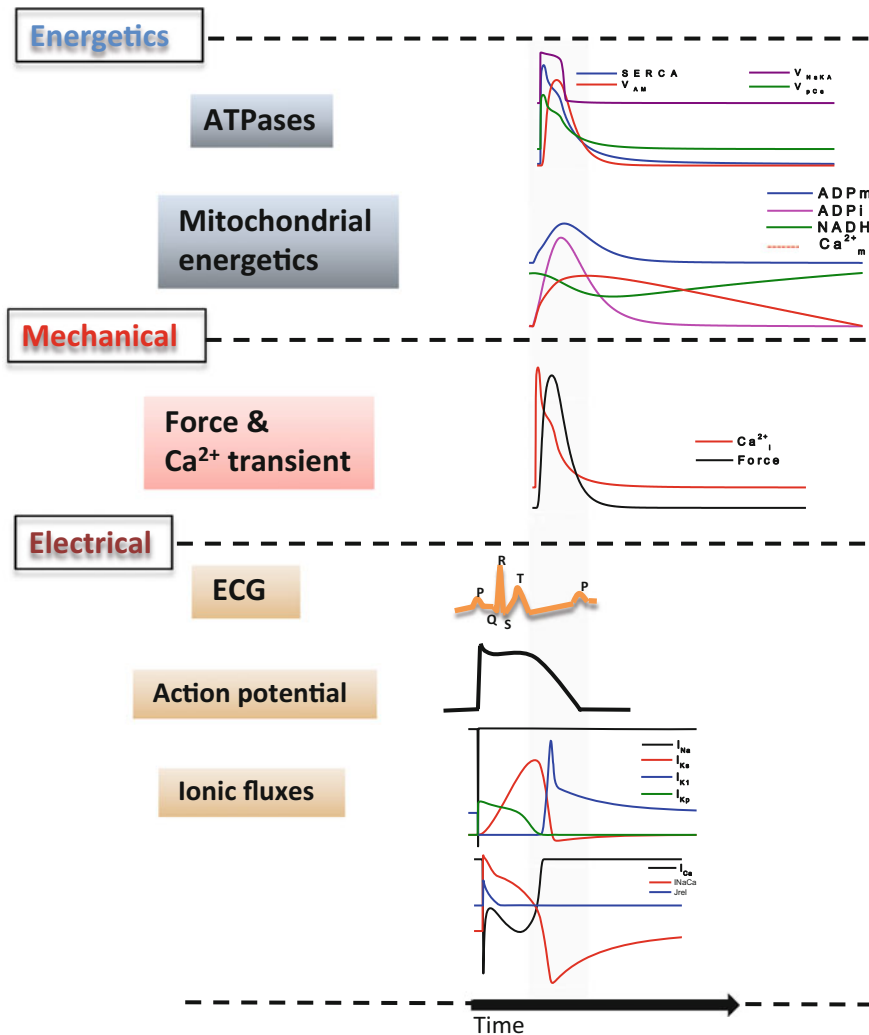


Fig. 5.1 Temporal unfolding of electrical, mechanical, and energetic processes during a single cardiomyocyte beat as computed by the Excitation–Contraction coupling Mitochondrial Energetic (ECME) model. The depolarization and repolarization phases of the action potential (AP) take place during the first 200 ms when the ECME model is stimulated every 2 s. This calculation reveals the multiple temporal scales involved. The *gray shaded* area is meant to highlight the earlier occurrence of electrical as compared with mechanical (contraction–relaxation) and metabolic/energetic processes. Mitochondrial energy fuels the electrical and contractile machinery of the heart cell on a slower time scale (few seconds) compared with the electrical processes (milliseconds), which are followed by mechanical events associated with the force of contraction and the Ca^{2+} transient

different compartments whose interaction is mediated by transport processes. If we zoom in within a set of processes we will find even more detailed networks, and the dynamics is reflected by fluxes occurring in different compartments, e.g., by channels and pumps in the plasma membrane, sarcoplasmic reticulum, myofibrils, and mitochondria.

The molecular view analyzes interactions in biomolecular networks involving different components which result in varied functional outputs: protein–protein, genetic expression (multi arrays), regulatory (protein–DNA interactions, combinatorial transcription factors), and signaling (signal transduction pathways through protein–protein and protein–small molecule interactions) (Cortassa et al. 2012).

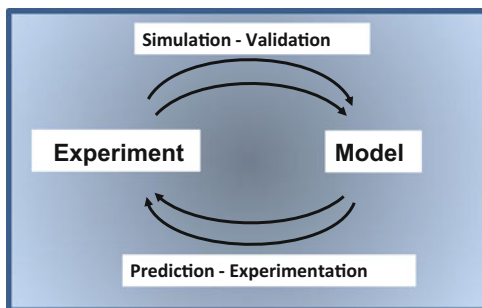
From a temporal perspective a highly tuned response exists in energy supply by mitochondria to the demand by electromechanical processes in the heart operating in the millisecond range (e.g., action potentials, calcium transients) (Fig. 5.1). This tight match between energy supply and demand can be more readily fulfilled by the highly synchronized and robust action of mitochondrial networks. In the heart, mitochondria constitute an extensive subcellular network, which occupies ~30 % of the heart cell volume, and appears to be wrapped by the sarcoplasmic reticulum and in close vicinity with the myofilaments and t-tubules. During maximal workload, the whole ATP pool in the heart cell is turned over in a few seconds, while ~2 % of that pool is consumed in each heartbeat. Both constancy and flexibility are required from the mitochondrial network in response to the changing metabolic demand for supplying a steady output of ATP to fuel contraction, and to adapt the rate of energy provision. Whereas under normal physiological conditions the availability of energy is fine-tuned to match changes in energy demand, under stress this is not the case.

The idea that mitochondria may function as a coordinated network of oscillators emerged from studies on living cardiomyocytes subjected to metabolic stress. The network behavior of mitochondria depends on local as well as global coordination in the cell, and ROS-induced ROS release is a mechanism that was shown to exert both local and cell-wide influence on the network. Mitochondrial network organization may be also essential for the temporal organization of the heart rhythm.

Mitochondrial network energetics, or the functioning of mitochondria as networks, represents an advantageous behavior for its coordinated action, under normal physiology, provides overall and usual robustness despite occasional failure in a few nodes, and improves energy supply during a swiftly changing demand (Aon and Cortassa 2012). Mitochondrial network energetics along with its remarkable nonlinear properties together with those of the whole heart itself set the stage for the appearance of critical phenomena and bifurcations leading to self-organized, emergent behavior. An amazing example of the latter is given by the existence, at critical points (mitochondrial criticality), of emergent macroscopic self-organized behavior escalating from the subcellular to the whole heart, eventually leading to the death of the animal. The demonstration of the involvement of mitochondrial oscillations in reperfusion-related arrhythmias after ischemic injury, and of their

Fig. 5.2 The experimental—computational synergy

The experimental – computational synergy



Synergy = reciprocal potentiation in successive iterative loops

pharmacological reversion, blunting oscillations, and stabilizing the action potential in different animal models, is strong proof of the involvement of the network behavior of mitochondrial energetics.

5.1 Experimental–Computational Synergy

In the next sections we will delineate the powerful synergy arising from a combined experimental and theoretical approach to unravel mechanisms underlying complex dynamic behavior. Specifically, we will describe how the interaction of computational modeling and experimental work led to the vision of mitochondria behaving as networks in architectural, topological, and dynamic senses. We also explore the physiological and pathophysiological consequences of the network behavior of mitochondrial function.

Figure 5.2 shows an overall flow diagram of the experimental–computational synergy. The main driving force underlying the synergy is the continual interaction between experiment and computational model which gives rise to iterative loops. The intrinsic dynamic of these loops works as follows: a model is validated as can be judged from its ability to simulate experimental results; this triggers model prediction of new, unexpected behavior which elicits experimental verification, followed by the discovery of novel properties revealed by the experiments which in turn feedback on the model that can be tested again in its ability to simulate them. If the model is unable to simulate the new behavior, then modifications (changes either in the structure of the model, or in the rate expressions or just in parameter values) are introduced. These changes may take the form of model upgrades to account for new processes, or different functional relationships between the model components already in place.

The iterative dynamic of the *experiment* ↔ *model* loop represents the synergy through theoretical prediction that works as a hypothesis-driven experimental test,

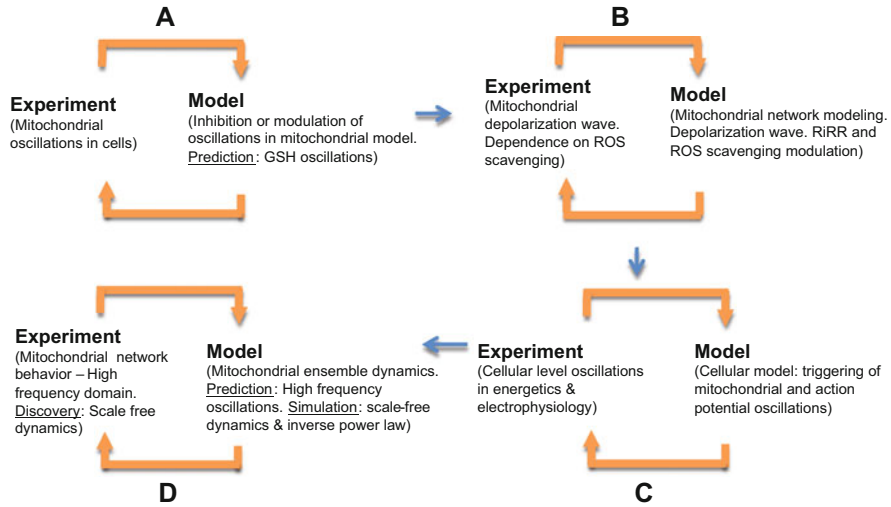


Fig. 5.3 Overview of the experimental—computational synergy as applied to the elucidation of the mechanisms involved in mitochondrial oscillations in the heart, and the discovery of scale-free dynamics in the mitochondrial network

and the results of which then become a new functional/mechanistic insight into the behavior of the experimental system. The loop can then reiterate from novel behavior as experimentally verified, and this can subsequently be further investigated in order to see if the model in its present form can account for the new phenomena. If not, then the model is further refined and upgraded.

5.2 Oscillatory Phenomena in Cardiomyocytes: A Case Study of Experimental–Modeling Synergy

In order to show how the experimental–computational synergy can be used to address a specific biological problem, we analyze the experimental demonstration of cell-wide mitochondrial oscillations in living cardiomyocytes (Figs. 5.3 and 5.4). To understand the mechanism underlying the oscillations, we developed a computational model of the mitochondrial oscillator (Cortassa et al. 2004). One of the aims of this modeling was to investigate the role of ROS in the mitochondrial oscillations described in living cardiomyocytes subjected to oxidative stress (Aon et al. 2003).

In the heart, under normal physiological conditions, the availability of energy is fine-tuned to match changes in energy demand. However, under stress this is not the case. Metabolically stressful conditions such as substrate deprivation, or oxidative stress, represent a pathophysiological situation under which mitochondrial

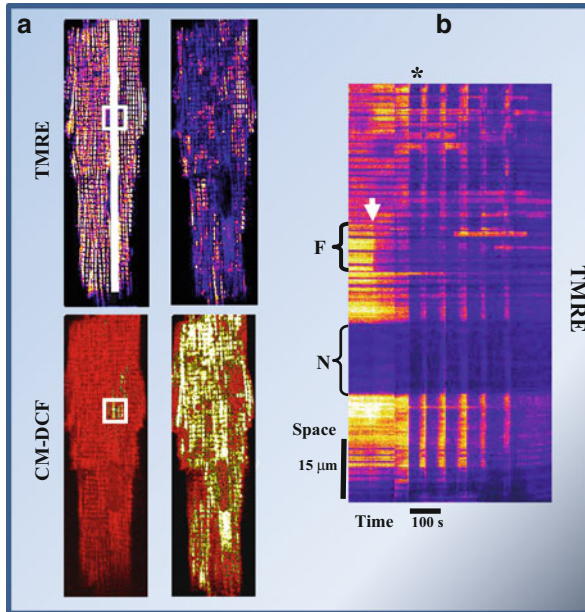


Fig. 5.4 Cell-wide synchronized mitochondrial oscillations after local generation of ROS. (a) Cardiomyocyte loaded at 37 °C with tetramethylrhodamine ethyl ester (TMRE, $\Delta\Psi_m$ indicator, upper images) and 5-(6)-chloromethyl-2, 7-dichloro-7-hydroxyfluorescein diacetate (CM-H₂DCFH, ROS-sensitive, lower images). By using two-photon laser excitation, and after 10–20 control images were collected, a small region of a cardiac myocyte (20 × 20 pixels) was excited in a single flash resulting in rapid loss of mitochondrial membrane potential, $\Delta\Psi_m$ (a, white square in upper left; b, white arrow) and local generation of ROS (a, white square in lower left). Thereafter, $\Delta\Psi_m$ remained depolarized in the flashed area throughout the experiment (see b). The right images in a show the first whole-cell $\Delta\Psi_m$ depolarization (b, asterisk) after a delay time. (b) Time-line image of TMRE created by analyzing a line drawn along the longitudinal axis of the cell (shown in a, upper left). The arrow points out the timing of the flash and the brackets point out the flash region (Upper) and the nucleus (Lower). The synchronous $\Delta\Psi_m$ mitochondrial oscillations are evident as vertical blue bands. The mitochondria that do not belong to the spanning cluster remained visibly polarized. Reproduced from Aon MA, Cortassa S, and O’Rourke B. (2004) PNAS 101, 4447–4452

energetics oscillates. Under these conditions the performance mode of mitochondrial function becomes a key arbiter of life and death at cellular and organ levels (Aon et al. 2006a; Gustafsson and Gottlieb 2008; O’Rourke et al. 2005). The idea that mitochondria could function as a coordinated network of oscillators emerged from studies in living cardiomyocytes subjected to metabolic stress (Aon et al. 2003, 2004a, 2006b).

5.2.1 Experimental Studies: A Brief Phenomenological Description of Mitochondrial Oscillations

The mitochondrial oscillator was first described experimentally under pathophysiological conditions of metabolic stress, e.g., substrate deprivation (Romashko et al. 1998), or oxidative stress (Aon et al. 2003). The mechanisms underlying the synchronization and propagation of mitochondrial oscillations in intact cardiomyocytes were explored in detail employing two-photon laser scanning fluorescence microscopy (Aon et al. 2003).

Experimentally, oscillations were triggered in a reproducible manner, a key for studying the underlying mechanisms under controlled conditions. Two-photon microscopy gives a detailed spatial picture of the mitochondrial network as can be seen in Fig. 5.4, in which a freshly isolated cardiomyocyte loaded with membrane potential and ROS sensors is shown. The fluorescence spatiotemporal dynamics along a line drawn throughout the longitudinal axis of an individual cell can be obtained. A time-line image of fluorescence intensity of TMRM or CM-DCF results in 2D plots that contain the whole spatial and temporal information of the stack of images. In these pseudo-color plots the blue bars correspond to mitochondrial membrane potential ($\Delta\Psi_m$) depolarization, and the yellow zones in between to $\Delta\Psi_m$ repolarization. These 2D plots clearly show that while the oscillations affect the whole cell, the flashed zone remains depolarized with high ROS (Fig. 5.4), and oxidized NADH (not shown) (Aon et al. 2003). After about 1 min, whole-cell mitochondrial oscillations are triggered whereby both $\Delta\Psi_m$ and the reduced state of NADH are synchronized into phase; with each $\Delta\Psi_m$ depolarization an associated burst in the rate of ROS production occurs.

5.2.2 Modeling Studies: A Brief Description of the Mitochondrial Oscillator

A model describing mitochondrial energetics and Ca^{2+} handling (Cortassa et al. 2003) was extended to describe the key features of the proposed mechanism of mitochondrial oscillations based on our experimental findings (Cortassa et al. 2004). The addition to this model of a leak of electrons from the respiratory chain to produce the free radical superoxide, $\text{O}_2^{\cdot-}$, as previously proposed for an outwardly rectifying inner membrane anion channel (IMAC) modeled after the centum pS channel in which conductance is $\text{O}_2^{\cdot-}$ activated (Borecky et al. 1997), and a cytoplasmic ROS scavenging system in the cytoplasm, was sufficient to support limit-cycle oscillations within certain parametric domains of our model (Cortassa et al. 2004). The normal anion permeability of IMAC would permit the passage of $\text{O}_2^{\cdot-}$ from the matrix to the cytoplasmic side of the inner membrane. In addition, the IMAC opening probability was assumed to be increased by $\text{O}_2^{\cdot-}$ at an external site.

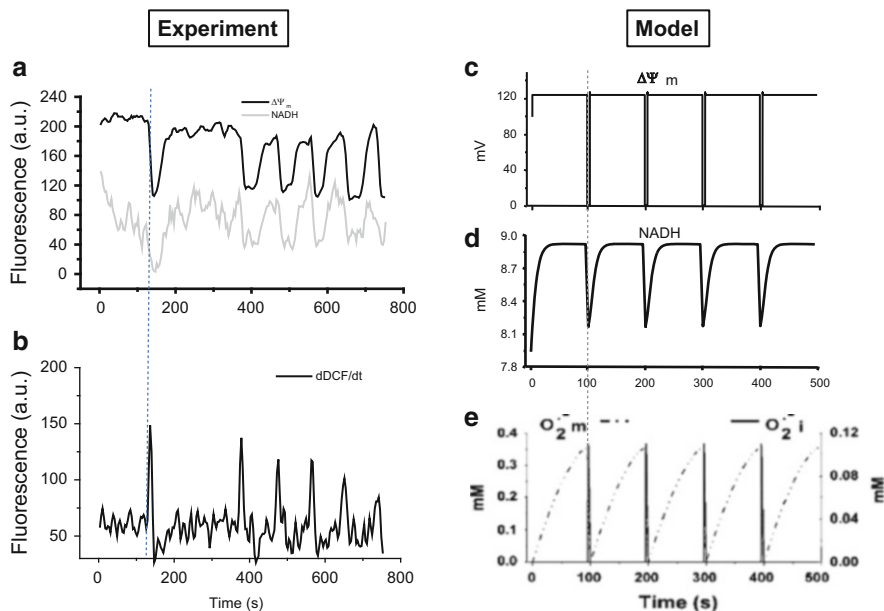


Fig. 5.5 Dynamic behavior of energetic and redox variables during mitochondrial oscillations (**a**, **b**) Shown is the simultaneous recording of the average whole-cell fluorescence of TMRE (a probe of $\Delta\Psi_m$) and NADH (autofluorescence) (**a**), and the rate of ROS accumulation (first derivative, $dDCF/dt$, of the CM-DCF signal) (**b**). (**c–e**) These panels display the simulation of the experimentally observed oscillations in $\Delta\Psi_m$, (**c**) NADH (**d**), and ROS (**e**, superoxide, $O_2^{\cdot-}$, in the model) with a mitochondrial oscillator model. The dashed lines are meant to emphasize the phase relationship between the different signals in the experiment (**a**, **b**) and variables in the simulation (**c–e**). Notice that, in the experiment as well as in the simulation, the peak in ROS accumulation occurs concomitantly with $\Delta\Psi_m$ depolarization and NADH oxidation during the initial phase of the oscillation. The model simulation further shows that the spike of $O_2^{\cdot-}$ corresponds to the release of the free radical accumulated in the mitochondrial matrix. Panels **a**, **b** were modified from Aon, Cortassa, Marban, O'Rourke (2003) *J Biol Chem* 278, 44735–44. Panels **c–e** were reproduced from Cortassa, Aon, Winslow, O'Rourke (2004) *Biophys J* 87, 2060–73

According to the postulated mechanism, under oxidative stress, the enhanced ROS production from the electron transport chain leads to accumulation in the mitochondrial matrix to critical levels (Aon et al. 2003, 2004a), thereby triggering the opening of IMAC in a positive feedback loop (Cortassa et al. 2004). According to this model, a burst in cytoplasmic ROS accompanies $\Delta\Psi_m$ depolarization (Fig. 5.5) as a result of a mixed process of accelerated $O_2^{\cdot-}$ production occurring concomitantly with a sudden increase in mitochondrial respiration. A pulse of cytoplasmic $O_2^{\cdot-}$ is released (Aon et al. 2007a; Cortassa et al. 2004).

The mitochondrial oscillator behaves as a relaxation oscillator, composed of both slow (ROS accumulation in the mitochondrial matrix) and fast (the IMAC opening and rapid ROS release) processes (Fig. 5.5e).

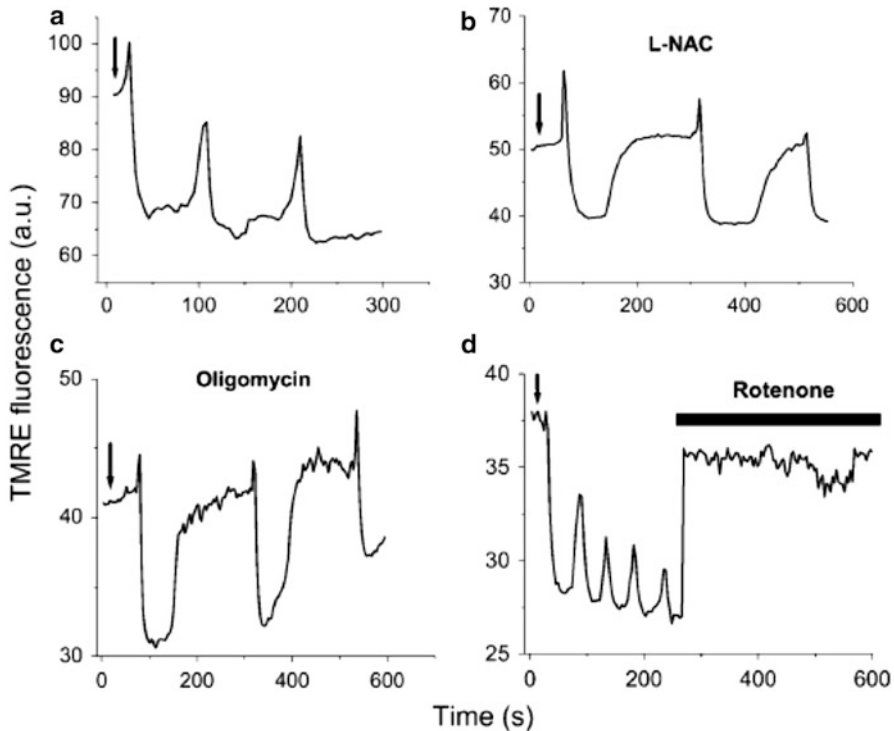


Fig. 5.6 Effects of scavengers or inhibitors of ROS production on mitochondrial oscillations. Recordings of the TMRE signal of myocytes showing cell-wide mitochondrial oscillations after a laser flash (arrows) in the absence (a) or in the presence of 4 mM *N*-acetyl-L-cysteine (L-NAC) for 30 min (b), or 10 µg/ml of oligomycin for 60 min (c), or after the acute addition of rotenone (15 µM) (d). Oscillations in mitochondrial metabolism were triggered as described in Fig. 5.4 (see also text). Reproduced from Cortassa, Aon, Winslow, O'Rourke (2004) *Biophys J* 87, 2060–73

5.3 First Iterative Loop: Cell-wide Mitochondrial Oscillations

Cell-wide synchronized oscillations in mitochondrial NADH, $\Delta\Psi_m$, and ROS could be reproducibly triggered by a focalized laser flash affecting only a few mitochondria (Fig. 5.4). We used two-photon scanning laser fluorescence microscopy and a laser flash to induce localized oxidative stress in a few mitochondria (~50). After a few seconds (~40 s on average), a synchronized cell-wide $\Delta\Psi_m$ depolarization occurred that extended and prolonged into cell-wide oscillations of the mitochondrial network in all tested energetic/redox variables ($\Delta\Psi_m$, NADH, ROS, GSH) (Figs. 5.4, 5.5, and 5.7).

We then concentrated on the cellular redox balance affecting the ROS production and ROS scavenging capacity of cells (Fig. 5.6). The oscillations could be slowed by increasing the ROS scavenging capacity of the cell (Fig. 5.6b), or by

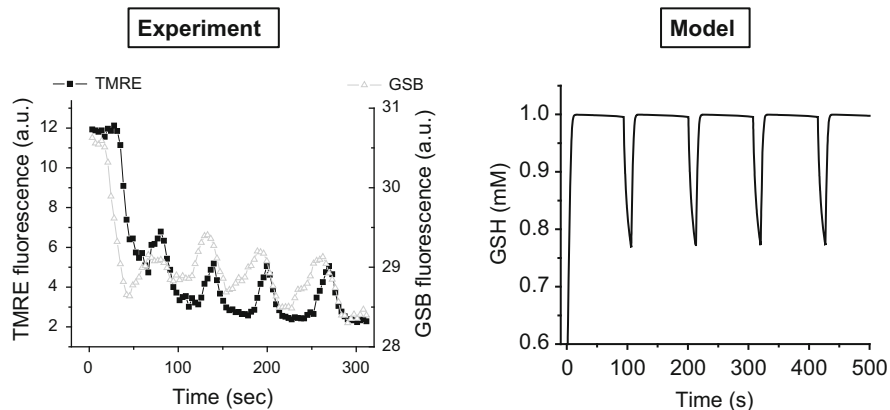


Fig. 5.7 Glutathione oscillations. (a) Experimental demonstration of GSH oscillations (70 s period) recorded simultaneously with $\Delta\Psi_m$. Oscillations were triggered after a localized laser flash as described in Fig. 5.4 in freshly isolated cardiomyocytes loaded with 100 nM tetramethylrhodamine methyl ester (TMRM) and 50 μM monochlorobimane, MCB (Cortassa et al. 2004). Reproduced from Cortassa, Aon, Winslow, O'Rourke (2004) *Biophys J* 87, 2060–73

blocking the mitochondrial ATP synthase (Fig. 5.6c). Mitochondrial oscillations could be interrupted by acute inhibition of mitochondrial ROS production (Fig. 5.6d), or by blockage of mitochondrial IMAC (Aon et al. 2003); these were later found to be activated under moderate oxidative stress (Aon et al. 2007b).

In the respiratory chain, oscillations were suppressed when we inhibited electron transfer complex I (rotenone), III (antimycin A/myxothiazol), or IV (cyanide), or the phosphorylation machinery F_1F_0 ATPase (oligomycin) or adenine nucleotide translocator (ANT, bongkreic acid). On the other hand, we reinforced the scavenging system of cardiac cells by adding a superoxide dismutase mimetic or N-acetyl cysteine (Aon et al. 2008a). Although we could suppress the mitochondrial oscillations by preincubation in the presence of ROS scavengers, it took much longer than respiratory inhibitors to see the effect (1–3 min vs. 1 h) (Aon et al. 2003). The scavengers also slowed the initial $\Delta\Psi_m$ depolarization wave (Aon et al. 2004a; Cortassa et al. 2004).

Model simulations showed the ability to reproduce the ~ 100 s oscillatory period and the phase relationship between $\Delta\Psi_m$ and NADH observed experimentally (Fig. 5.5). The model was also able to simulate other major experimental findings, including (1) the requirements of ROS to cross a threshold so as to trigger fast $\Delta\Psi_m$ depolarization, (2) the suppressive effect of inhibitors of the electron transport chain, adenine nucleotide translocator (ANT) and the F_1F_0 ATPase on ROS production and $\Delta\Psi_m$ oscillation (Cortassa et al. 2004), (3) the effects of anion channel inhibitors, and (4) the sensitivity of the oscillator to the level of ROS scavengers.

After validation, the model led to predictions that were tested in the experimental system. The model anticipated oscillatory behavior of reduced glutathione (GSH), and that was experimentally demonstrated as well as its phase relationship with $\Delta\Psi_m$ (Fig. 5.7) (Cortassa et al. 2004).

5.4 Second Iterative Loop: Mitochondrial Criticality and Network Redox Energetics During Oscillations

5.4.1 Mitochondrial Criticality

Under oxidative stress mitochondrial behavior reaches a critical point that we called *mitochondrial criticality* (Aon et al. 2004a), an emergent macroscopic response manifested as a generalized $\Delta\Psi_m$ collapse followed by synchronized oscillation in the mitochondrial network under stress (Fig. 5.4). As the mitochondria approach criticality, two main questions arise (Aon et al. 2006a): (1) how does the signal propagate throughout the network? and (2) how does $\Delta\Psi_m$ depolarization occur almost simultaneously in distant regions of the cell?

Applying percolation theory to the problem (see Box 5.1) we found that, prior to the first global $\Delta\Psi_m$ depolarization, approximately 60 % of the mitochondria had accumulated ROS to a level roughly 20 % above baseline (Aon et al. 2004a), which was the threshold for activation of the oscillator at the whole cell level. This critical density of mitochondria (60 %) was consistent with that predicted by percolation theory (Box 5.1). Moreover, the spatial distribution of mitochondria at the threshold exhibits a fractal dimension in agreement with theory (Aon et al. 2003, 2004b).

Beyond criticality, self-sustained oscillations in $\Delta\Psi_m$ continue as a consequence of a bifurcation in the dynamics of the system (Cortassa et al. 2004). However, the spatial pattern of subsequent depolarization of the network will typically follow that of the original percolation cluster, with some mitochondria always remaining outside the cluster. Another important feature of the percolation model is that the global transition can be prevented if the $O_2^{\cdot-}$ concentration reaching the neighboring mitochondrion is decreased below threshold, either by decreasing $O_2^{\cdot-}$ production (e.g., by inhibiting respiration), decreasing $O_2^{\cdot-}$ release (e.g., by inhibiting IMAC), or increasing the local ROS scavenging capacity (e.g., by increasing the GSH pool) (Aon et al. 2004a, 2007b; Cortassa et al. 2004).

Box 5.1: Standard 2D Percolation Theory as Applied to Explain Mitochondrial Criticality

Percolation describes how local neighbor–neighbor interactions among elements in a lattice can scale to produce a macroscopic response spanning from one end of the array to the other (Stauffer and Aharony 1994). Such a “spanning cluster” forms when there is a critical density of elements close to the threshold for a transition (the percolation threshold). Experimentally, the “spanning cluster” involved ~60 % of the mitochondrial lattice with increased levels of ROS (Aon et al. 2004a). This value was consistent with a critical density of mitochondria at the percolation threshold (p_c), which, for a square lattice in percolation theory, is equal to 0.593 or ~59 % (Feder 1988; Stauffer and Aharony 1994).

(continued)

Box 5.1 (continued)

Another signature feature of percolation processes at p_c is that they are organized as fractals. This property implies that local processes can scale to produce macroscopic behavior. At p_c , the mass of the spanning cluster increases with the size of the lattice, L , as a power law, L^{D_f} , with D_f as the fractal dimension (Feder 1988; Mandelbrot 1977; Stauffer and Aharony 1994). Fractal box counting analysis of our data yielded a fractal dimension of $D_f \sim 1.82$, close to that exhibited by percolation clusters and cytoskeletal lattices at p_c ($D_f \sim 1.90$) (Aon and Cortassa 1994, 1997; Aon et al. 2003; Feder 1988; Stauffer and Aharony 1994).

Several interesting properties of the mitochondrial response can be explained when the network is considered as a percolation cluster. First, the question of the limited diffusivity and lifetime of $O_2^{\cdot-}$ as the triggering molecule is answered, since the only relevant diffusion distance is the inter-mitochondrial spacing ($\sim 1 \mu\text{m}$). As long as there are enough neighboring mitochondria belonging to the spanning cluster (i.e., they have accumulated enough $O_2^{\cdot-}$ to approach the percolation threshold) an universal phase transition will occur (Feder 1988; Schroeder 1991; Stauffer and Aharony 1994) and mitochondria will depolarize for the first time throughout the cell (Aon et al. 2003, 2004a).

5.4.2 Modeling Mitochondrial Network Redox Energetics

The mitochondrial oscillator model utilized in the first iterative loop corresponds to an isolated mitochondrion representing the average behavior of the mitochondrial population, actually (in the case of the cardiomyocyte or cardiac cell) organized as a network. Therefore, accounting for the spatial relationships between individual mitochondria within the network became crucial to simulating the initial depolarization wave that signals the energetic collapse of the mitochondrial network. The importance of this seminal event in the escalation of failures, from mitochondria propagating to cells and groups of them, and finally attaining the whole heart, made it worthwhile (and in fact crucial) to unravel the fundamental mechanisms involved. More specifically, we wanted to explore whether a reaction–diffusion mechanism could be responsible of the spreading of failure of individual organelles to the whole cell. According to our model, wave propagation comprises the nonlinear dependence of an IMAC opening on $O_2^{\cdot-}$ accumulation in the matrix, and the free radical autocatalytic release and spreading in the network; we hypothesized that mechanistically this could be enough to reproduce the wave phenomenon and the underlying ROS-induced ROS release (RIRR).

In order to achieve this goal we developed a mathematical model of RIRR based on reaction–diffusion (RD-RIRR) in one- and two-dimensional mitochondrial

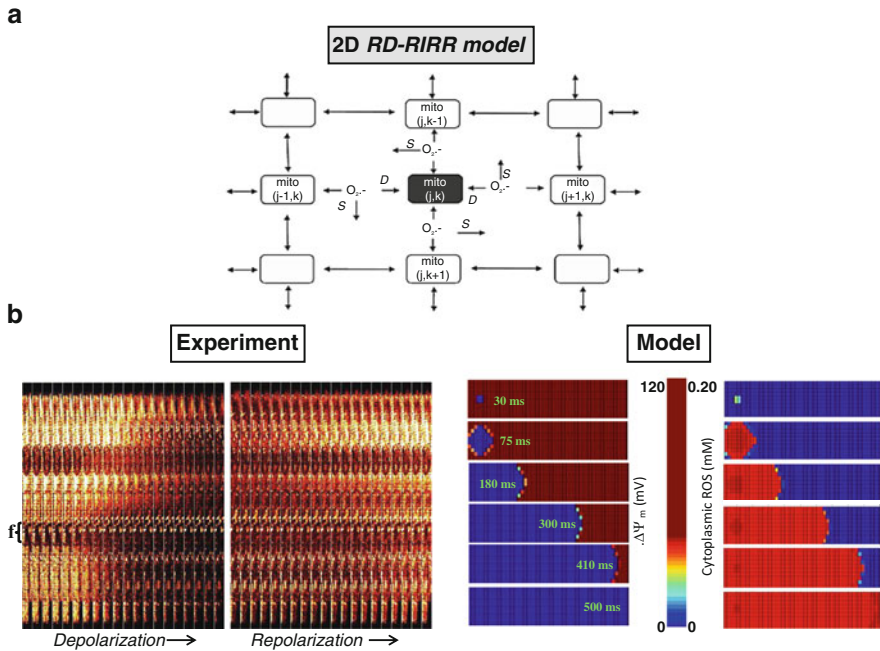


Fig. 5.8 Scheme of the RD-RIRR mitochondrial network model. In the two-dimensional RD-RIRR model neighboring mitochondria are chemically coupled with each other through superoxide anion, $O_2^{\cdot-}$, diffusion. *Light* and *dark gray* indicate polarized and depolarized mitochondria, respectively. *Arrows* indicate release of $O_2^{\cdot-}$ and its effect on mitochondrial neighbors. *D* stands for $O_2^{\cdot-}$ diffusion, and *S* for $O_2^{\cdot-}$ scavenging by Cu,Zn SOD and catalase. Reproduced from Zhou, Aon, Almas, Cortassa, Winslow, O'Rourke (2010) PLoS Computational Biology 6(1): e1000657. doi:10.1371/journal.pcbi.1000657

networks (see Box 5.2). The nodes of the RD-RIRR network are comprised of models of individual mitochondria that include a mechanism of ROS-dependent oscillation based on the interplay between ROS production, transport, and scavenging, and incorporating the tricarboxylic acid (TCA) cycle, oxidative phosphorylation, and Ca^{2+} handling. Local mitochondrial interaction is mediated by $O_2^{\cdot-}$ diffusion and the $O_2^{\cdot-}$ -dependent activation of IMAC (Fig. 5.8a).

In a 2D network composed of 500 mitochondria, model simulations reveal $\Delta\Psi_m$ depolarization waves similar to those observed when isolated guinea pig cardiomyocytes are subjected to local laser flash or antioxidant depletion (Fig. 5.8b).

Box 5.2: Accounting for ROS-Induced ROS Release Based on Reaction–Diffusion: Computational Model of a Network Comprised by 500 Mitochondria Based on the ROS-Dependent Mitochondrial Oscillator

The thin optical sectioning ability of two-photon laser scanning fluorescence microscopy can be used to examine the behavior of the mitochondrial network in a single plane of a cardiomyocyte (Fig. 5.4) (Aon et al. 2003, 2004a). To compare the experimental results obtained with optical imaging experiments in cardiomyocytes subjected to oxidative stress, a mitochondrial reaction–diffusion ROS-induced ROS release (RD-RIRR) computational model was developed. Each non-boundary node (mitochondrion) in the network was considered to have four nearest neighbors for $O_2^{\cdot-}$ interaction (Fig. 5.8). At each node (j, k) of the 2D network, $O_2^{\cdot-}$ dynamics is described by the mass balance equation based on $O_2^{\cdot-}$ reaction and diffusion (Zhou et al. 2010):

$$\frac{\partial C_{O_2-i}(x,y,t)}{\partial t} = D_{O_2-i} \left(\frac{\partial^2 C_{O_2-i}(x,t)}{\partial x^2} + \frac{\partial^2 C_{O_2-i}(y,t)}{\partial y^2} \right) + f(C_{O_2-i}, t)$$

$$\text{Boundary conditions: } \frac{\partial C_{O_2-i}(0,t)}{\partial x} = 0; \frac{\partial C_{O_2-i}(X,t)}{\partial x} = 0$$

$$\frac{\partial C_{O_2-i}(0,t)}{\partial y} = 0; \frac{\partial C_{O_2-i}(Y,t)}{\partial y} = 0$$

$$\text{Initial conditions: } C_{O_2-i}(x,y,0) = g(x,y)$$
(5.1)

where D_{O_2-i} is the cytoplasmic $O_2^{\cdot-}$ diffusion coefficient, X and Y indicate the total lengths in the dimensions x and y , respectively, and $f(C_{O_2-i}, t) = Vt_{O_2-i}(t) - VSOD_{O_2-i}(t)$. Vt_{O_2-i} is the rate of $O_2^{\cdot-}$ transport (release) from the mitochondrion (via IMAC), and $VSOD_{O_2-i}$, the $O_2^{\cdot-}$ scavenging rate by Cu, Zn superoxide dismutase (SOD). The function $g(x,y)$ describes the distribution of $O_2^{\cdot-}$ at time 0 (the initial condition). The spatial coordinates, x and y , are subjected to discretization to numerically solve the system by the finite difference method. Non-flux boundary conditions were used.

To solve this large nonlinear network consisting of 500 (50×10) mitochondria (each node described by 15 state variables), a high-performance parallel computer was used. To be suitable for parallel computation, Eq. (5.1) was rewritten in the matrix form using forward Euler method to approximate the time derivative of C_{O_2-i} at each node (j, k) :

$$C_{O_2-i}(j, k, t + \Delta t) = C_{O_2-i}(j, k, t) + [\text{Diff}_{O_2-i}(j, k, t) + f(C_{O_2-i}(j, k, t))] \Delta t$$

(continued)

Box 5.2 (continued)

Reaction–diffusion theory (pioneered by Turing (1952)), as a basis for pattern formation in biological or chemical systems, emphasizes the importance of two components; an autocatalytic reaction producing a local product (mediator or ‘morphogen’ as originally defined by Turing), and the transport of this product by diffusion away from the source. This process can give rise to spontaneous symmetry-breaking and the appearance of self-organized spatial patterns including waves and oscillations (Aon et al. 1989; Cortassa et al. 1990; Meinhardt 1982; Nicolis and Prigogine 1977). With respect to the present model, the reaction consists of the reduction of O_2 to produce ROS (specifically $O_2^{\cdot-}$) driven by mitochondrial electron donors (e.g., NADH). The local concentration of $O_2^{\cdot-}$ around the mitochondrion is shaped by several other factors, including buffering by the antioxidant reactions and transport of $O_2^{\cdot-}$ across the mitochondrial membrane. Diffusion of the $O_2^{\cdot-}$ to neighboring mitochondria is shaped by the $O_2^{\cdot-}$ diffusion coefficient, $D_{O_2^{\cdot-}}$, and the amount of the $O_2^{\cdot-}$ scavenger enzyme superoxide dismutase present, which consequently determines the rate of propagation of $\Delta\Psi_m$ depolarization through the network. As expected, increasing SOD concentration slowed down the depolarization wave.

The rate of propagation of the depolarization wave in the model corresponded to $26 \mu\text{m s}^{-1}$ with low $D_{O_2^{\cdot-}}$ (of the order of $10^{-14} \text{cm}^2 \text{s}^{-1}$), which compares well with the experimentally determined $22 \mu\text{m s}^{-1}$ at 37°C (Aon et al. 2004a). A restricted diffusion range of $O_2^{\cdot-}$ in cells is consistent with experimental data; however, the actual diffusion coefficient of $O_2^{\cdot-}$ in cells (with antioxidant systems disabled) has not been determined and is likely to be influenced by local reactions with other molecules and molecular crowding around mitochondria, which would decrease the effective volume, increase the viscosity of the medium, and increase collision probability. This assumption of restricted diffusion is represented by the low $D_{O_2^{\cdot-}}$ in the model.

5.4.3 *Experimental–Theoretical Test of a Main Mechanistic Assumption of Mitochondrial Oscillations: Superoxide as a Trigger of $\Delta\Psi_m$ Depolarization*

The original ROS-dependent mitochondrial oscillator model (Cortassa et al. 2004) considered cytoplasmic $O_2^{\cdot-}$ as the primary ROS that would increase IMAC open probability in an autocatalytic process. H_2O_2 was ruled out because it had been shown experimentally that superoxide dismutase mimetics, which should enhance H_2O_2 accumulation, in fact suppressed the oscillations in $\Delta\Psi_m$ (Aon et al. 2003). To test the assumption that $O_2^{\cdot-}$ could directly trigger IMAC opening, we applied increasing concentrations of potassium superoxide (KO_2 , an $O_2^{\cdot-}$ donor) to partially permeabilized myocytes. Increasing the exogenous cytoplasmic KO_2

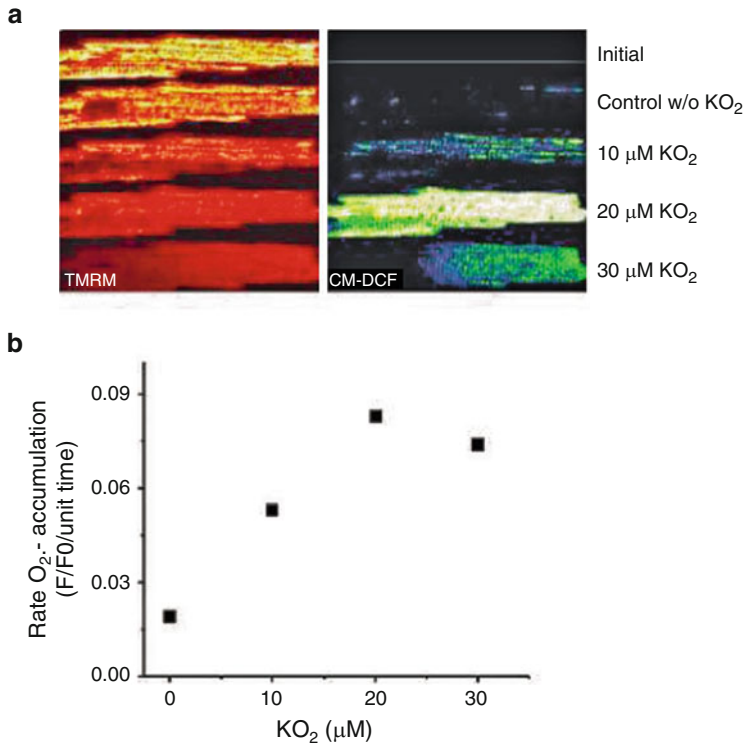


Fig. 5.9 Mitochondrial $O_2^{\cdot-}$ and $\Delta\Psi_m$ in response to increased exogenous $O_2^{\cdot-}$. Myocytes were loaded with TMRM (100 nM) and CM-H₂DCFDA (2 μ M) for at least 20 min and imaged using two-photon laser scanning fluorescence microscopy. After loading, the excess dye was washed out and the cells were briefly superfused with a permeabilizing solution (saponin) (Aon et al. 2007). After permeabilization, the myocytes were continuously perfused with an intracellular solution containing GSH:GSSG at a ratio of 300:1. The TMRM was included in the medium to avoid depletion of the probe during depolarization–repolarization cycles. **(a)** The TMRM and CM-DCF images of a permeabilized cardiomyocyte at time zero after loading and before (*top row image*) or after permeabilization and 5 min imaging under control conditions (Control, *second row*) or the presence of KO_2 , an $O_2^{\cdot-}$ donor (10 μ M, *third row*; 20 μ M, *fourth row*; 30 μ M, *fifth row*), after 3 min equilibration in each case. RIRR-mediated $\Delta\Psi_m$ depolarization without a permeability transition occurs at the two lower concentrations, while loss of the CM-DCF probe (\sim 500 MW) from the mitochondrial matrix due to PTP opening occurs at 30 μ M KO_2 . **(b)** The rates of $O_2^{\cdot-}$ accumulation as a function of KO_2 concentration. Slopes were calculated when the linear rate of change of the CM-DCF signal stabilized under each condition. Reproduced from Zhou, Aon, Almas, Cortassa, Winslow, O’Rourke (2010) PLoS Computational Biology 6(1): e1000657. doi:10.1371/journal.pcbi.1000657

concentration, from 10 to 20 μ M, elicited progressive $\Delta\Psi_m$ depolarization and increased the rate of mitochondrial $O_2^{\cdot-}$ accumulation (Fig. 5.9b). Exposure of the cell to 30 μ M KO_2 induced an irreversible collapse of $\Delta\Psi_m$, accompanied by the

complete release of the $O_2^{\cdot-}$ sensor, indicative of permeability transition pore (PTP) opening (Fig. 5.9a).

5.4.4 Propagation of Depolarization Through ROS-Induced ROS Release (RIRR)

RIRR as the basic mechanism of propagation of $\Delta\Psi_m$ depolarization and $O_2^{\cdot-}$ release was also demonstrated in the 2D RD-RIRR mitochondrial network model (Zhou et al. 2010). Consisting of five hundred (10×50) mitochondria, the 2D RD-RIRR model was parametrically initialized to represent a condition of high oxidative stress to simulate a mitochondrial network at criticality. Approximately 1 % (6 out of 500) of the mitochondrial network was induced to undergo depolarization (Fig. 5.8b). A local increase in $O_2^{\cdot-}$ concentration and depolarization of $\Delta\Psi_m$ in this area was evident, similar to those processes observed in experiments in which we applied a localized laser flash to a fraction of the mitochondrial network (Fig. 5.4). $\Delta\Psi_m$ depolarization propagated outward in all directions from the six perturbed mitochondria and then appeared as a longitudinal wave as the edges of the array were encountered (Fig. 5.8b, model left panel). Importantly, a wave of increased $O_2^{\cdot-}$ accompanied the $\Delta\Psi_m$ depolarization wave (Fig. 5.8b, model right panel).

Moreover, the model further contributed to our understanding by showing that (1) local gradients of cytoplasmic $O_2^{\cdot-}$, determined by diffusion and scavenger capacity, play a significant role in determining the rate of propagation of the $\Delta\Psi_m$ depolarization and repolarization waves; and (2) by uncovering a novel aspect of the synchronization mechanism, i.e., that clusters of mitochondria that are in a state characteristic of the oscillatory domain of the parametric space can entrain mitochondria that would otherwise display stable dynamics (Zhou et al. 2010).

While focusing on a specific mechanism of RIRR (i.e., IMAC-mediated), the model results provided general theoretical support for mitochondrial communication occurring by way of $O_2^{\cdot-}$ diffusion. The RD-RIRR model simulations confirm that $O_2^{\cdot-}$ diffusion occurring locally between neighboring mitochondria over a distance of a few microns is sufficient for propagation and synchronization of $\Delta\Psi_m$ depolarization over a larger distance (Aon et al. 2004a; Zhou et al. 2010).

5.5 Third Iterative Loop: Mitochondrial Network Redox Energetics Escalates from Subcellular to Cellular Level

The experimental studies had shown that laser flash-induced cell-wide mitochondrial oscillations in isolated cardiomyocytes produced shortening of the cellular action potential (AP) (Akar et al. 2005; Aon et al. 2003). The collapse of $\Delta\Psi_m$

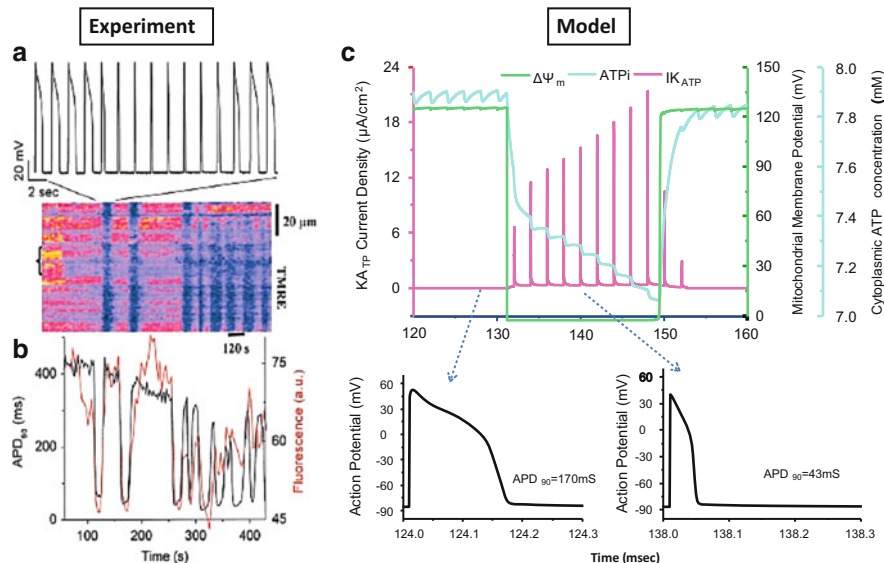


Fig. 5.10 Effects of mitochondrial oscillation on the electrical excitability of the cardiomyocyte (a) Action potentials (AP, upper panel) evoked by brief current injections were recorded in current clamp mode during whole-cell patch clamp while simultaneously imaging $\Delta\Psi_m$ with TMRE (lower panel). During a synchronized cell-wide depolarization–repolarization cycle, the AP shortened in synchrony with fast mitochondrial depolarization, and the cell became unexcitable in the fully depolarized state (remaining upward spikes are from the stimulus only). Recovery of $\Delta\Psi_m$ coincided with restoration of AP. (b) Temporal correlation between the AP duration at 90 % repolarization and $\Delta\Psi_m$. The current–voltage relationship of the oscillatory membrane current fits the profile of the sarcolemmal K_{ATP} current (Aon et al. 2003). (c) Simulations of $\Delta\Psi_m$, cytoplasmic ATP concentration ([ATP]_i) and sarcolemmal K_{ATP} current during oscillations triggered by oxidative stress, and comparison of APs during polarized and depolarized states. Modified from Aon, Cortassa, Marban, O’Rourke (2003) *J Biol Chem* 278, 44735–44, and Zhou, Cortassa, Wei, Aon, Winslow, O’Rourke (2009) *Biophys J* 97, 1843–1852

triggered by ROS was shown experimentally to be coupled to the opening of sarcolemmal ATP-sensitive potassium (K_{ATP}) channels, contributing to electrical dysfunction during ischemia–reperfusion. K_{ATP} channels have a low open probability under physiological conditions, but are rapidly activated during ischemia or metabolic inhibition (Lederer et al. 1989; Noma 1983).

Figure 5.10 shows that during the depolarized phase of the oscillation, the AP interval shortens as a consequence of the activation of sarcolemmal K_{ATP} currents rendering the myocyte electrically inexcitable during the nadir of $\Delta\Psi_m$ (Akar et al. 2005; Aon et al. 2003). The fact that these effects were mediated by $\Delta\Psi_m$ depolarization was indicated by inhibition of the IMAC-mediated mitochondrial oscillations with 4’-chlorodiazepam (4’-Cl-DZP) an intervention that concomitantly reestablished and stabilized the sarcolemmal AP.

Highly nonlinear interactions are involved in the mitochondrial oscillation-driven inexcitability of the cardiac cell, including communication through transport

between different subcellular compartments and processes of different nature, i.e., metabolic and electromechanical (Fig. 5.1). A comprehensive mathematical model represents an invaluable tool for addressing this problem. Coupling between the mitochondrial energy state and electrical excitability mediated by the sarcolemmal K_{ATP} current ($I_{K,ATP}$) was incorporated into a computational model of excitation–contraction coupling linked to mitochondrial bioenergetics, and accounting for mitochondrial RIRR.

The model at this stage produced results that were very similar to the experimental observations. During the phase of mitochondrial depolarization, the AP shortened by almost 75% (Fig. 5.10) and the intracellular Ca^{2+} transient amplitude and force production decreased (Zhou et al. 2009). Mitochondrial depolarization accelerates K_{ATP} current activation because the decreased $\Delta\Psi_m$ causes the ATP synthase to run in reverse, thus consuming cytoplasmic ATP and decreasing the phosphorylation potential. Tight coupling between the mitochondrial energy state and the sarcolemmal K_{ATP} current is facilitated by the high-energy phosphoryl transfer reactions of the cytoplasm (Cortassa et al. 2006; Dzeja and Terzic 2003; Sasaki et al. 2001; Zhou et al. 2009). Most importantly, whole-cell model simulations demonstrated that increasing the fraction of oxygen diverted from the respiratory chain to ROS production triggers limit-cycle oscillations of $\Delta\Psi_m$, redox potential, and mitochondrial respiration through the activation of the ROS-sensitive IMAC.

5.6 Fourth Iterative Loop: Scale-Free Dynamics of Mitochondrial Network Redox Energetics

Another model prediction concerned the oscillatory frequency as a function of the superoxide dismutase (SOD) activity. This prediction resulted from stability analysis of the model that showed amplitude and frequency modulation of oscillations when the balance of ROS was changed by increasing SOD (Fig. 5.11). In the absence of metabolic stress, cardiomyocytes loaded with tetramethylrhodamine methyl ester (TMRM, $\Delta\Psi_m$ fluorescent reporter) display stable $\Delta\Psi_m$ for more than an hour. Using two-photon scanning laser fluorescence microscopy, cells were imaged every 110 ms and the average fluorescence from the whole or part of the network, calculated.

Applying power spectral analysis (PSA) and relative dispersional analysis (RDA) to $\Delta\Psi_m$ time series we found that, collectively, cardiac mitochondria behave as a highly correlated network of oscillators (see Box 5.3). PSA revealed that the ensemble of oscillators represented by the mitochondrial network exhibits many frequencies across temporal scales, spanning from milliseconds to minutes. This behavior corresponds to scale-free dynamics, mathematically characterized by an inverse power law when represented in a log–log plot of power versus frequency (Fig. 5.12; see also Boxes 5.3 and 5.4). The power spectrum followed a homogeneous inverse power law of the form $1/f^\beta$ with $\beta \sim 1.7$ (Aon et al. 2006b).

The origins of the inverse power law behavior exhibited by mitochondrial network dynamics

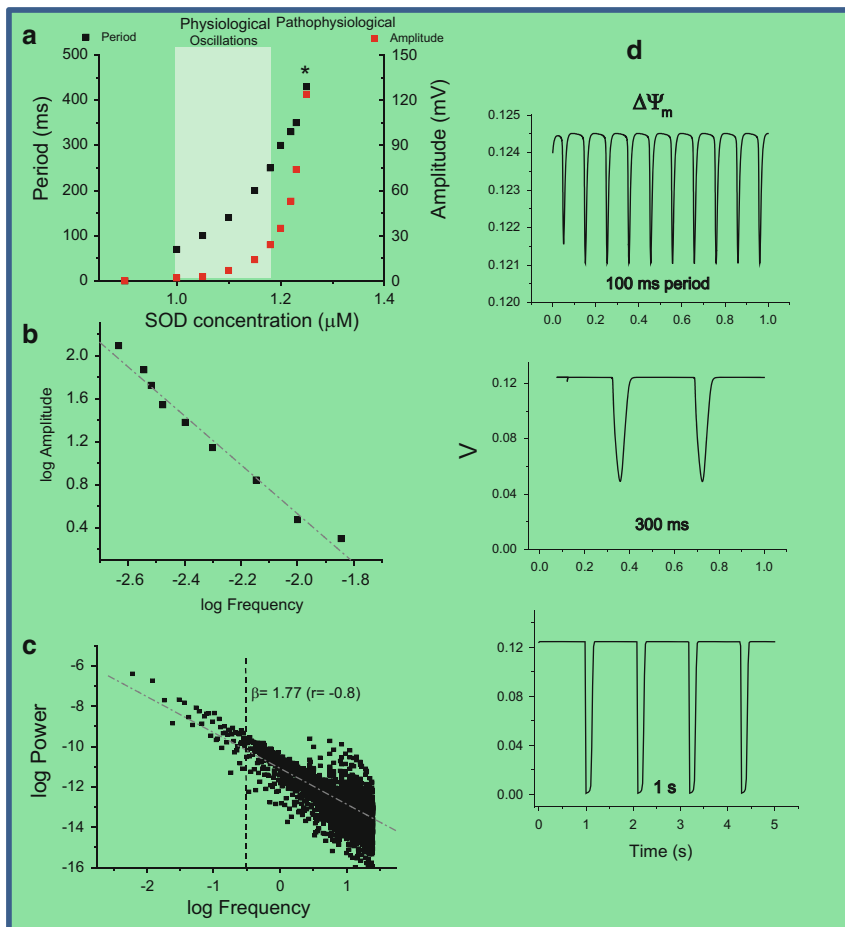


Fig. 5.11 Modulation of the oscillation period by the rate of ROS scavenging through SOD, and inverse power law behavior of the amplitude versus frequency relationship exhibited by the mitochondrial oscillator. (a) Oscillations with different periods and amplitude in $\Delta\Psi_m$ were simulated with our computational model of the mitochondrial oscillator by changing SOD concentration (Cortassa et al. 2004). (b) The double log graph of the amplitude versus frequency (1/period) was plotted from $\Delta\Psi_m$ oscillations with amplitudes in the range of 2–124 mV and periods ranging from 70 to 430 ms, respectively (see Aon et al. 2006, and their Supplemental Material for more details). (c, d) From the simulations, we selected five oscillatory periods in the high-frequency domain (between 70 and 300 ms) and one from the low-frequency (1-min period) domain and attributed each one of them proportionally to a network composed by 500 mitochondria as described in Aon et al. (2006). A matrix containing a total of 500 columns (mitochondria) and 6,000 rows was constructed. The time steps represented by the rows correspond to a fixed integration step of 20 ms for the numerical integration of the system of ordinary differential equations. We applied RDA and PSA to the average value of each row of the matrix at, e.g., time 1, T1, that represents the experimental average value of fluorescent intensity of the $\Delta\Psi_m$ probe (corresponding to mV) obtained every 110 ms from 500 mitochondria (on average) from each image of our stack

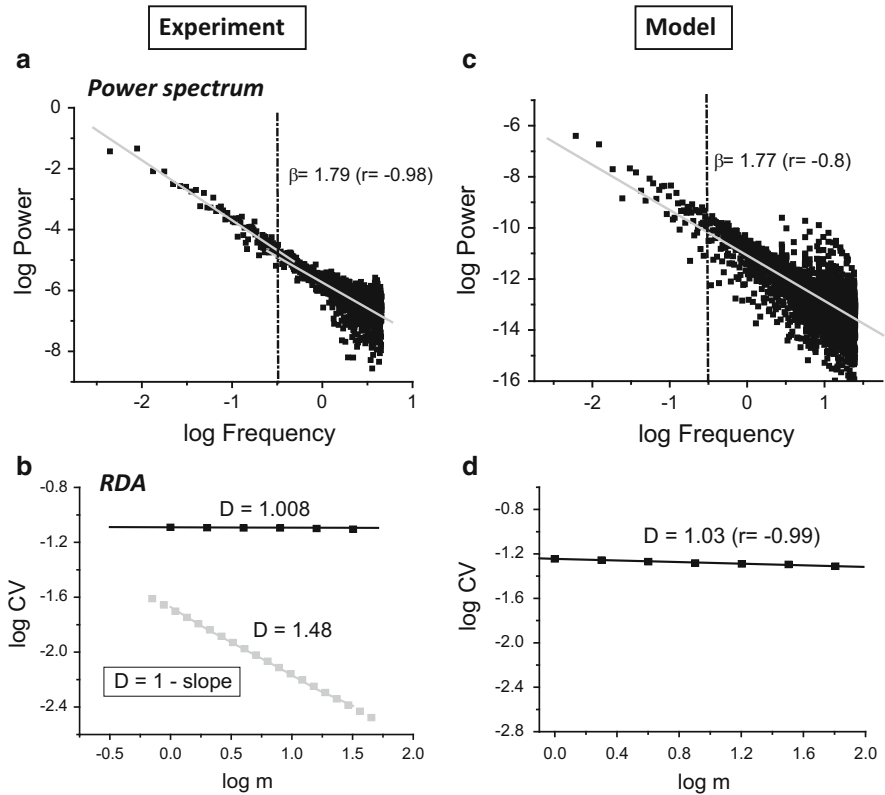


Fig. 5.12 Experimental evidence and model simulation of the inverse power law behavior observed after RDA or PSA of the fluorescence time series of TMRM. Mathematical procedures and simulations were performed as described in Boxes 5.3 and 5.4, and Fig. 5.11

RDA unveiled the existence of long-term temporal correlation (“memory”) among oscillators in the network (Fig. 5.12; see also Box 5.3). This led us to conclude that the behavior in the physiological domain is also oscillatory but with low-amplitude high-frequency oscillations. These results also indicated that the oscillators are weakly coupled by low levels of mitochondrial ROS in the high-frequency domain. We considered the behavior under these conditions to belong to the “physiological” state, because fluctuations at high-frequency (but restricted amplitude) range imply depolarization only of between microvolts to a few millivolts (Fig. 5.11) (Aon et al. 2006b). Decreasing mitochondrial ROS production at the level of the respiratory chain, or blocking the ROS-induced ROS release (R-IRR) mechanism by inhibiting the mitochondrial benzodiazepine receptor in the physiological domain, consistently diminished the extent of correlated behavior of the mitochondrial network in the high-frequency domain (Aon et al. 2006b).

Under metabolic stress, however, an imbalance between production and scavenging can take ROS over a threshold resulting in strong coupling between mitochondria through RIRR (Figs. 5.4 and 5.8) (Aon et al. 2003; Zorov et al. 2000). When subjected to these challenging stressful conditions, the mitochondrial network spontaneously organizes into a synchronized cluster with a dominant low-frequency high-amplitude oscillation that spans the whole cell (Aon et al. 2004a, 2006b). The RIRR mechanism is effective locally, but long-range synchronization is due to the attainment of criticality by ~60 % of mitochondria that form a cluster, the “spanning cluster”, across the cardiomyocyte. Mitochondria belong to the “spanning cluster” when ROS (more specifically, O_2^-) attain a threshold in the matrix, after which $\Delta\Psi_m$ depolarization ensues, triggering a similar response in neighboring mitochondria.

Underlying the inverse power law behavior observed experimentally in the power spectrum is the inverse relationship found in the model simulations of the double log plot of amplitude versus frequency (Fig. 5.11). Two key factors contribute to this dependence—the superoxide dismutase (SOD) activity and the balance between the rate of ROS production and scavenging. In the oscillatory domain, an increase in the SOD rate results in longer periods and higher amplitude oscillations (Fig. 5.11).

We hypothesized that if, according to the experimental results, the mitochondrial network were exhibiting a mixture of frequencies, then we should be able to simulate the inverse power law behavior obtained by either PSA or RDA (see Box 5.4). To test this hypothesis we simulated five different oscillatory periods ranging from 70 ms to 300 ms and one long period (1 min) oscillation (Fig. 5.11). A combination of 80 % short-period and 20 % long-period oscillations allowed us to simulate the inverse power law behavior observed experimentally by either PSA or RDA (Fig. 5.12). This result demonstrated that mixing a relatively few (six) periods of limit-cycle type of oscillation is enough to explain our experimental data. Using a similar approach, we were also able to simulate the transition from physiological to pathophysiological behavior (Aon et al. 2006b). This transition, according to simulations, and in agreement with experimental data, is effected when at least 60 % of the mitochondrial network dynamics is dominated by the long period, high-amplitude $\Delta\Psi_m$ oscillations (Fig. 5.12) ((Aon et al. 2006b), and their Supplementary Material).

Box 5.3: Fast Fourier Transform (FFT) Is a Key Mathematical Procedure Utilized in Power Spectral Analysis (PSA)

FFT of a time series enables the statistical determination of the power (equivalent to the amplitude squared) of each frequency component of a signal. When this analytical procedure was applied to the time series of $\Delta\Psi_m$ from the mitochondrial network, a large number of frequencies in multiple timescales became evident (Aon et al. 2006b, 2008b). Thus,

(continued)

Box 5.3 (continued)

statistically, the mitochondrial network rather than exhibiting a single “characteristic” frequency shows multiple frequencies, typical of *dynamic fractals*.

Fractals possess a two-sided nature both as geometric (spatial) and as dynamic objects. This trait enables techniques commonly applied for characterization and quantification of fractals in the spatial domain to be applied to describe dynamic behavior. The different spatial and temporal scales displayed by an object (be it a shape or a time series) can be quantified by lacunarity, a mass-related statistical parameter quantified by the coefficient of variation or relative dispersion, RD (= standard deviation (SD)/mean). RD is a strong function of scale (Aon and Cortassa 2009) that in the case of self-similar time series or “dynamic fractals” remains constant (i.e., the object looks the same at all scales) (West 1999). The determination of RD at successively larger intervals from a time series constitutes the basic mathematical procedure for applying relative dispersion analysis (RDA). RDA of $\Delta\Psi_m$ time series from the mitochondrial network revealed long-term temporal correlations (“memory”).

Box 5.4: Simulation of the Inverse Power Law Behavior Exhibited by the Mitochondrial Network of Cardiomyocytes

From the simulations, we selected five oscillatory periods in the high-frequency domain (between 70 and 300 ms) and one from the low-frequency (1 min period) domain and attributed each one of them proportionally to a network composed of 500 mitochondria (i.e., every 100 mitochondria will oscillate with the same period). This number of mitochondria is similar to that present in a single optical slice of a cardiomyocyte (~1 μm focal depth) that we analyze by two-photon laser scanning microscopy with 110 ms/frame time resolution. Our experimental results could be precisely simulated with a mixture of 80 % short-period and 20 % long-period oscillations.

According to this protocol, we then constructed a matrix: with mitochondria in columns, and time, T_i , on rows. The final matrix contained a total of 500 columns and 6,000 rows. The time steps represented by the rows correspond to a fixed integration step of 20 ms for the numerical integration of the system of ODEs. The fixed integration step of 20 ms was chosen for the simulation of all periods within the range of 70–300 ms and 1 min in order to avoid aliasing effects.

	Mito1	Mito2	Mito3	...Mito _n
T_0				
T_1				
T_2				
... T_n				

5.7 Mitochondrial Oscillations in the Intact Heart: Testing the Consequences of Mitochondrial Criticality

We determined if the nonlinear oscillatory phenomena described in single cells can be observed at the level of the whole heart. Studies performed in permeabilized cardiomyocytes revealed that the critical state can be induced by partial depletion of the GSH pool and that the reversible (IMAC-mediated) and irreversible (PTP-mediated) depolarization of $\Delta\Psi_m$ can be distinguished from the cytoplasmic glutathione redox status. IMAC-mediated $\Delta\Psi_m$ oscillation was triggered at a GSH/GSSG ratio of 150:1–100:1, whereas PTP opening is triggered at a GSH/GSSG of 50:1 (Aon et al. 2007b). These results pointed out that GSH and probably also the glutathione redox potential are the main cellular variables that determine the approach of the mitochondrial network to criticality through an increase in oxidative stress by the overwhelming of the antioxidant defenses.

Extending the mechanistic findings in permeabilized cardiomyocytes (Aon et al. 2007b) to the mitochondrial ROS-dependent oscillator described in living cardiac myocytes (Aon et al. 2003, 2004a), and computational models (Cortassa et al. 2004) to the level of the myocardial syncytium, we showed that mitochondrial $\Delta\Psi_m$ oscillations could be triggered by ischemia/reperfusion (I/R) or GSH depletion in intact perfused hearts using two-photon scanning laser microscopy (Slodzinski et al. 2008). These results confirmed that the appearance of oscillatory behavior is not restricted to isolated cardiomyocytes but also happens in the epicardium of intact hearts (either flash-triggered or GSH depletion elicited), in both $\Delta\Psi_m$ and NADH (Fig. 5.13).

An important prediction of the percolation model utilized to explain the mechanism of mitochondrial synchronization at criticality is that the global transition can be prevented if the $O_2^{\cdot-}$ concentration reaching the neighboring mitochondrion is decreased below threshold. This can be accomplished either by decreasing $O_2^{\cdot-}$ production (inhibiting respiration), decreasing $O_2^{\cdot-}$ release (inhibiting IMAC), or increasing the local ROS scavenging capacity (increasing the GSH pool) (Aon et al. 2004a, 2007b; Cortassa et al. 2004). Within this rationale, $\Delta\Psi_m$ depolarization induced by depleting the GSH pool could induce cardiac arrhythmias even under normoxic conditions (Aon et al. 2007b, 2009). Indeed, Brown et al. (2010) demonstrated that systematic oxidation of the GSH pool with diamide in Langendorff-perfused guinea pig hearts elicited ventricular fibrillation under normoxia (Fig. 5.14b, d). Experimental evidence further indicating the involvement of IMAC was noted when the arrhythmias induced by GSH depletion (Brown et al. 2010) or H_2O_2 -elicited oxidative stress (Biary et al. 2011) were prevented with the IMAC blocker 4'-Cl-DZP (Fig. 5.14c, e).

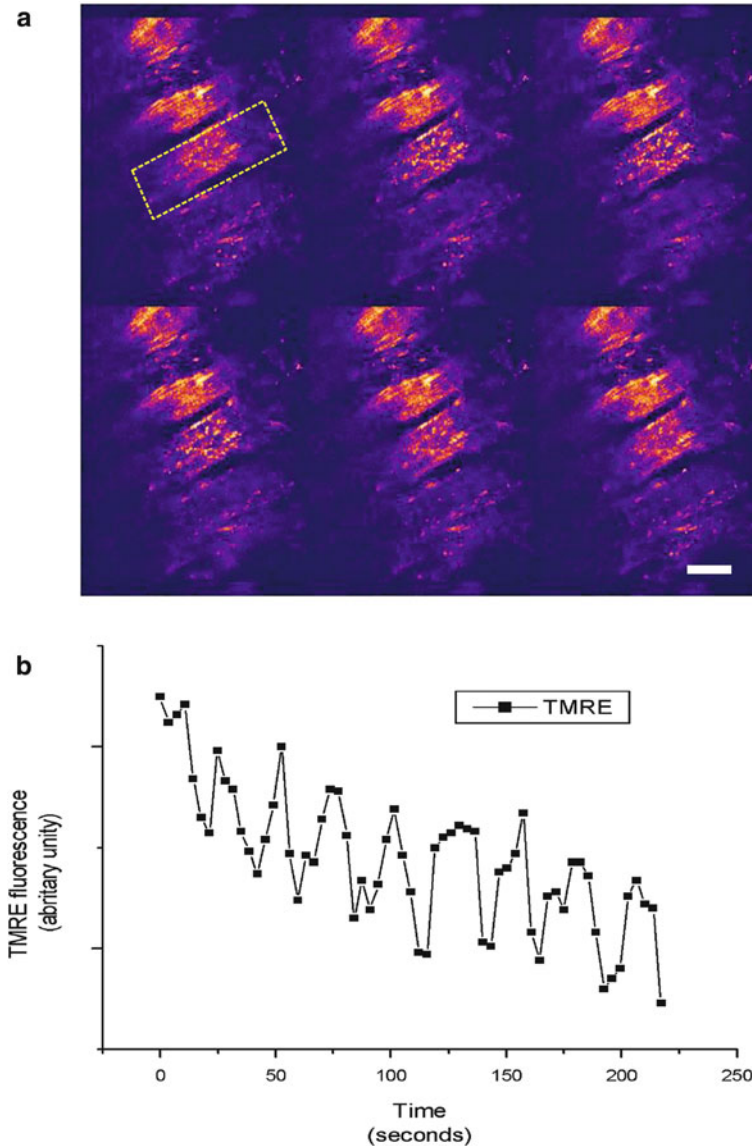


Fig. 5.13 Mitochondrial membrane potential oscillations in myocytes of the intact heart. **(a, b)** After 2–3 min of normoxic perfusion with Ca^{2+} -free Tyrode's buffer, the $\Delta\Psi_m$ signal (TMRE fluorescence) became unstable and spontaneous oscillations were observed. Sustained oscillations in $\Delta\Psi_m$ were observed for several minutes in the cell indicated by the *yellow dashed line* in panel **a**. Both intracellular and intercellular heterogeneity of $\Delta\Psi_m$ is evident in the epicardial optical sections. *Scale bar* in **a** equals 20 μm . Reproduced from Slodzinski, Aon, O'Rourke (2008) *J Mol Cell Cardiol* 45, 650–660

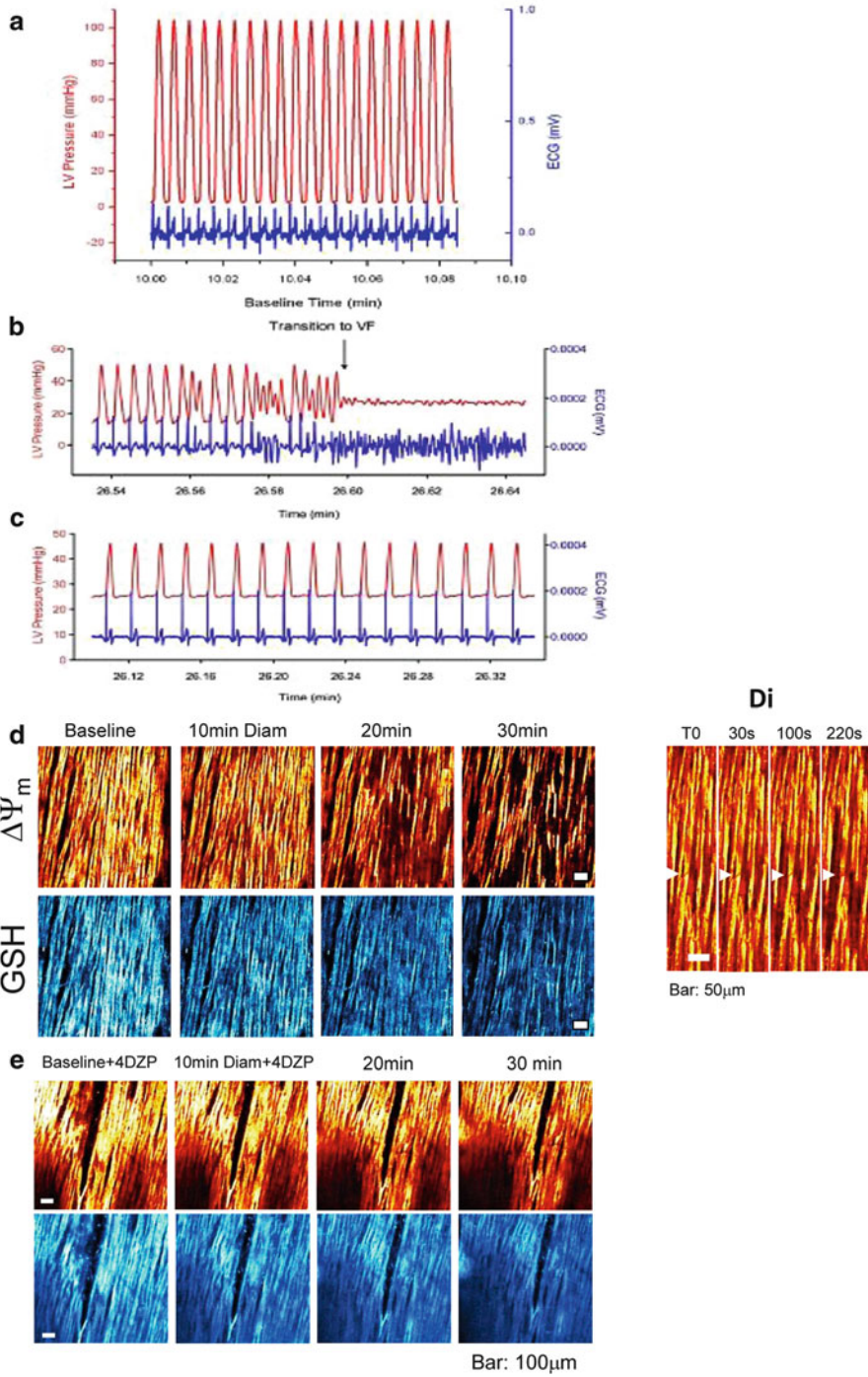


Fig. 5.14 Representative LV pressure and ECG from guinea pig heart. **(a)** Control heart after 10 min of baseline perfusion with simultaneous left ventricular (LV), pressure (*red*), and

5.8 New Modeling Developments Along the Experimental–Computational Synergy

The latest version of the isolated mitochondrion model—the mitochondrial energetic-redox (ME-R) model—includes all four main redox couples NADH/NAD⁺, NADPH/NADP⁺, GSH/GSSG, and Trx(SH)₂/TrxSS together with a complete array of antioxidant defenses. All four variables are considered as present in two compartments: matrix and extra-mitochondrial; the latter compartment comprising intermembrane space and cytoplasm (Kembro et al. 2013). Also taken into account are the NADP⁺-dependent **isocitrate dehydrogenase** (IDH2) in the TCA cycle, and transhydrogenase (THD), two of the three main NADPH sources in mitochondria. The Trx system involves thioredoxin reductase and peroxiredoxin whilst the glutaredoxin system accounts for the recovery of glutathionylated proteins (using GSH as cofactor), superoxide dismutases (SOD) (matrix-located MnSOD and extra-mitochondrial Cu,ZnSOD), and catalase activity also in the extra-mitochondrial compartment.

The model by Kembro et al. (2013) has been formulated on the basis of our mitochondrial energetics version that included pH regulation, ion dynamics (H⁺, Ca²⁺, Na⁺, Pi), respiratory fluxes from complex I and II, tricarboxylic acid cycle (TCA cycle) dynamics, adenine nucleotide exchange (ANT), and ATP synthesis (Wei et al. 2011).

The qualitative dynamic behavior exhibited by the new ME-R model reveals that, as in former versions (Cortassa et al. 2004; Zhou et al. 2009), the underlying oscillatory mechanism involves ROS imbalance determined by the interplay between ROS production and scavenging as the main trigger of oscillations. This happens irrespective of the bi-compartmental nature of the ME-R model, accounting for ROS scavenging in both the matrix and extra-mitochondrial space.

5.9 Conclusions

Experimental–computational synergy involves the reciprocal potentiation of the loop involving experimental work and mathematical modeling that operates iteratively via the multiple simulation–validation and prediction–experimentation

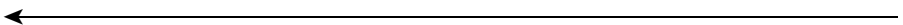


Fig. 5.14 (continued) electrocardiogram (ECG, blue). **(b)** LV pressure and ECG in a heart during diamide treatment showing the transition to ventricular fibrillation (VF, blue) with concomitant loss of pump function (red). **(c)** LV pressure and ECG in a heart during diamide treatment plus 64 μM 4'-CIDzp. **(d, e)** Simultaneous imaging of $\Delta\Psi_m$ (top) and GSH (bottom) in intact guinea pig hearts using two-photon microscopy after exposure to diamide (D) and diamide + 4' chlorodiazepam, 4'-CIDzp (e). The inset Di shows in detail the propagation of $\Delta\Psi_m$ depolarization in the syncytium at the cardiomyocyte level. Reproduced from Brown, Aon, Frasier, Sloan, Maloney, Anderson, O'Rourke (2010) J Mol Cell Cardiol 48, 673–679

loops. When applied systematically and rigorously the synergetic loop of experiment-model enables a deeper understanding of complex biological phenomena as shown in this chapter. Thorough application of this strategy both enabled us to formulate the following new concepts and to unravel complex emergent phenomena exhibited by networks of metabolic and electromechanical processes in the cardiac cell:

- Mitochondria are organized as a dynamic network of oscillators in the cardiac myocyte
- The mitochondrial network is synchronized by ROS to different degrees of coupling strength, either weakly or strongly during physiological or pathophysiological behavior, respectively.
- The mitochondrial network is embedded within other metabolic networks of the cardiac cell, thereby interacting with metabolic, electrical, and mechanical processes.
- Emergent phenomena take place in these networks in the form of physiologically normal long-term correlations involving signaling processes, or as failures that can propagate from the subcellular to the whole heart producing potentially catastrophic arrhythmias (see Chap. 10).
- Striking similarities between the cardiac redox control systems and those in the evolutionarily distant organism, baker's yeast (*Saccharomyces cerevisiae*), indicate an ancient commonality of central core metabolic mechanisms (see Chap. 12), and how a mutually enhanced understanding of these can be gleaned from comparative studies of different biological systems (Aon et al. 2007c, 2008b; Lemar et al. 2007; Lloyd et al. 2012).

Acknowledgments This work was performed with the financial support of R21HL106054 and R01-HL091923 from NIH.

References

- Akar FG, Aon MA, Tomaselli GF, O'Rourke B (2005) The mitochondrial origin of postischemic arrhythmias. *J Clin Invest* 115:3527–35
- Aon MA, Cortassa S (1994) On the fractal nature of cytoplasm. *FEBS Lett* 344:1–4
- Aon MA, Cortassa S (1997) Dynamic biological organization. *Fundamentals as applied to cellular systems*. Chapman & Hall, London
- Aon MA, Cortassa S (2009) Chaotic dynamics, noise and fractal space in biochemistry. In: Meyers R (ed) *Encyclopedia of complexity and systems science*. Springer, New York
- Aon MA, Cortassa S (2012) Mitochondrial network energetics in the heart. *Wiley Interdiscip Rev Syst Biol Med* 4:599–613
- Aon M, Thomas D, Hervagault JF (1989) Spatial patterns in a photobiochemical system. *Proc Natl Acad Sci USA* 86:516–9
- Aon MA, Cortassa S, Marban E, O'Rourke B (2003) Synchronized whole cell oscillations in mitochondrial metabolism triggered by a local release of reactive oxygen species in cardiac myocytes. *J Biol Chem* 278:44735–44

- Aon MA, Cortassa S, O'Rourke B (2004a) Percolation and criticality in a mitochondrial network. *Proc Natl Acad Sci USA* 101:4447–52
- Aon MA, O'Rourke B, Cortassa S (2004b) The fractal architecture of cytoplasmic organization: scaling, kinetics and emergence in metabolic networks. *Mol Cell Biochem* 256–257:169–84
- Aon MA, Cortassa S, Akar FG, O'Rourke B (2006a) Mitochondrial criticality: a new concept at the turning point of life or death. *Biochim Biophys Acta* 1762:232–40
- Aon MA, Cortassa S, O'Rourke B (2006b) The fundamental organization of cardiac mitochondria as a network of coupled oscillators. *Biophys J* 91:4317–27
- Aon MA, Cortassa S, Lemar KM, Hayes AJ, Lloyd D (2007a) Single and cell population respiratory oscillations in yeast: a 2-photon scanning laser microscopy study. *FEBS Lett* 581:8–14
- Aon MA, Cortassa S, Maack C, O'Rourke B (2007b) Sequential opening of mitochondrial ion channels as a function of glutathione redox thiol status. *J Biol Chem* 282:21889–900
- Aon MA, Cortassa S, O'Rourke B (2007a) On the network properties of mitochondria. Wiley-VCH, p 111–35
- Aon MA, Cortassa S, O'Rourke B (2008a) Mitochondrial oscillations in physiology and pathophysiology. *Adv Exp Med Biol* 641:98–117
- Aon MA, Roussel MR, Cortassa S, O'Rourke B, Murray DB, Beckmann M, Lloyd D (2008b) The scale-free dynamics of eukaryotic cells. *PLoS One* 3:e3624
- Aon MA, Cortassa S, Akar FG, Brown DA, Zhou L, O'Rourke B (2009) From mitochondrial dynamics to arrhythmias. *Int J Biochem Cell Biol* 41:1940–8
- Biary N, Xie C, Kauffman J, Akar FG (2011) Biophysical properties and functional consequences of reactive oxygen species (ROS)-induced ROS release in intact myocardium. *J Physiol* 589:5167–79
- Borecky J, Jezek P, Siemen D (1997) 108-pS channel in brown fat mitochondria might be identical to the inner membrane anion channel. *J Biol Chem* 272:19282–9
- Brown DA, Aon MA, Frasier CR, Sloan RC, Maloney AH, Anderson EJ, O'Rourke B (2010) Cardiac arrhythmias induced by glutathione oxidation can be inhibited by preventing mitochondrial depolarization. *J Mol Cell Cardiol* 48:673–9
- Cortassa S, Sun H, Kernevez JP, Thomas D (1990) Pattern formation in an immobilized bienzyme system. A morphogenetic model. *Biochem J* 269:115–22
- Cortassa S, Aon MA, Marban E, Winslow RL, O'Rourke B (2003) An integrated model of cardiac mitochondrial energy metabolism and calcium dynamics. *Biophys J* 84:2734–55
- Cortassa S, Aon MA, Winslow RL, O'Rourke B (2004) A mitochondrial oscillator dependent on reactive oxygen species. *Biophys J* 87:2060–73
- Cortassa S, Aon MA, O'Rourke B, Jacques R, Tseng HJ, Marban E, Winslow RL (2006) A computational model integrating electrophysiology, contraction, and mitochondrial energetics in the ventricular myocyte. *Biophys J* 91:1564–89
- Cortassa S, Aon MA, Iglesias AA, Aon JC, Lloyd D (2012) An introduction to metabolic and cellular engineering, 2nd edn. World Scientific, Singapore
- Dzeja PP, Terzic A (2003) Phosphotransfer networks and cellular energetics. *J Exp Biol* 206:2039–47
- Feder J (1988) *Fractals*. Plenum, New York
- Gustafsson AB, Gottlieb RA (2008) Heart mitochondria: gates of life and death. *Cardiovasc Res* 77:334–43
- Kembro JM, Aon MA, Winslow RL, O'Rourke B, Cortassa S (2013) Integrating mitochondrial energetics, redox and ROS metabolic networks: a two-compartment model. *Biophys J* 104:332–343
- Lederer WJ, Nichols CG, Smith GL (1989) The mechanism of early contractile failure of isolated rat ventricular myocytes subjected to complete metabolic inhibition. *J Physiol* 413:329–49
- Lemar KM, Aon MA, Cortassa S, O'Rourke B, Muller CT, Lloyd D (2007) Diallyl disulphide depletes glutathione in *Candida albicans*: oxidative stress-mediated cell death studied by two-photon microscopy. *Yeast* 24:695–706

- Lloyd D, Cortassa S, O'Rourke B, Aon MA (2012) What yeast and cardiomyocytes share: ultradian oscillatory redox mechanisms of cellular coherence and survival. *Integr Biol (Camb)* 4:65–74
- Mandelbrot BB (1977) *The fractal geometry of nature*. W.H. Freeman, New York
- Meinhardt H (1982) *Models of biological pattern formation*. Academic, London
- Nicolis G, Prigogine I (1977) *Self-organization in nonequilibrium systems : from dissipative structures to order through fluctuations*. Wiley, New York, p 491
- Noma A (1983) ATP-regulated K⁺ channels in cardiac muscle. *Nature* 305:147–8
- O'Rourke B, Cortassa S, Aon MA (2005) Mitochondrial ion channels: gatekeepers of life and death. *Physiology (Bethesda)* 20:303–15
- Romashko DN, Marban E, O'Rourke B (1998) Subcellular metabolic transients and mitochondrial redox waves in heart cells. *Proc Natl Acad Sci USA* 95:1618–23
- Sasaki N, Sato T, Marban E, O'Rourke B (2001) ATP consumption by uncoupled mitochondria activates sarcolemmal K(ATP) channels in cardiac myocytes. *Am J Physiol Heart Circ Physiol* 280:H1882–8
- Schroeder M (1991) *Fractals, chaos, power laws. Minutes from an infinite paradise*. W.H. Freeman and Company, New York
- Slodzinski MK, Aon MA, O'Rourke B (2008) Glutathione oxidation as a trigger of mitochondrial depolarization and oscillation in intact hearts. *J Mol Cell Cardiol* 45:650–60
- Stauffer D, Aharony A (1994) *Introduction to percolation theory*. Taylor & Francis, London
- Turing AM (1952) The chemical basis of morphogenesis. *Phil Trans R Soc Lond B* 237:37–72
- Wei AC, Aon MA, O'Rourke B, Winslow RL, Cortassa S (2011) Mitochondrial energetics, pH regulation, and Ion dynamics: a computational-experimental approach. *Biophys J* 100: 2894–903
- West BJ (1999) *Physiology, promiscuity and prophecy at The Millennium: A tale of tails*. World Scientific, Singapore
- Zhou L, Cortassa S, Wei AC, Aon MA, Winslow RL, O'Rourke B (2009) Modeling cardiac action potential shortening driven by oxidative stress-induced mitochondrial oscillations in guinea pig cardiomyocytes. *Biophys J* 97:1843–52
- Zhou L, Aon MA, Almas T, Cortassa S, Winslow RL, O'Rourke B (2010) A reaction–diffusion model of ROS-induced ROS release in a mitochondrial network. *PLoS Comput Biol* 6: e1000657
- Zorov DB, Filburn CR, Klotz LO, Zweier JL, Sollott SJ (2000) Reactive oxygen species (ROS)-induced ROS release: a new phenomenon accompanying induction of the mitochondrial permeability transition in cardiac myocytes. *J Exp Med* 192:1001–14